J Solid State Electrochem (2018) 22:1–9
DOI 10.1007/s10008-017-3712-2

ORIGINAL PAPER

Effect of crystallite size on the intercalation pseudocapacitance of lithium nickel vanadate in aqueous electrolyte

Haritha Hareendrakrishnakumar[1] · **Reshma Chulliyote**[1] · **Mary Gladis Joseph**[1]

Received: 24 April 2017 / Revised: 30 June 2017 / Accepted: 24 July 2017 / Published online: 3 August 2017

Abstract This work describes lithium nickel vanadate ($LiNiVO_4$) as a pseudocapacitor electrode material for the first time. The micro and nano-sized $LiNiVO_4$ are synthesized via mechanochemical reaction and hydrothermal reaction followed by calcination, respectively. The phase purity, surface morphology and microstructure of the $LiNiVO_4$ synthesized by both methods are analysed by X-ray diffraction and scanning electron microscopy techniques. The lithium ion intercalation-extraction behaviour of the $LiNiVO_4$ electrode material is investigated in 1 M LiOH electrolyte solution. The results demonstrate an improved capacitive performance for nano-sized $LiNiVO_4$ electrode synthesized via hydrothermal reaction due to the collective effect of small size and additional redox sites. The nanocrystalline $LiNiVO_4$ electrode exhibits a high specific capacitance of 456.56 F g^{-1} at a current density of 0.5 A g^{-1}. The cycle stability test reveals exceptional capacitance retention of 99.60% even after 1000 cycles owing to the unique structural feature which permit intercalation mechanism. These findings demonstrate the significance of lithium transition metal vanadate-based electrode material in the development of lithium ion intercalation pseudocapacitors.

Keywords Ternary metal oxide · Mechanochemical synthesis · Hydrothermal synthesis · Electrochemical reactions · Crystallite size · Pseudocapacitor

✉ Mary Gladis Joseph
marygladis@iist.ac.in; jmarygladis@gmail.com

[1] Department of Chemistry, Indian Institute of Space Science and Technology, Valiyamala, Thiruvananthapuram 695547, India

Introduction

Supercapacitors, also termed as electrochemical capacitors, have attracted tremendous attention as potential devices for future electrochemical energy storage due to their high power density, long cycling life, fast charge/discharge process and environmental friendliness [1–4]. The electrode material is one of the vital factors to improve the electrochemical performance of supercapacitors. In common, the electrode materials can be classified as carbon-based materials, conducting polymer materials and transition metal oxides. However, lower specific capacitance of carbon-based materials and the mechanical degradation of conducting polymers very much limit their application as electrode materials [5]. Transition metal oxides have been widely explored as potential electrode materials for supercapacitors because of the ease of large-scale fabrication and their multiple redox reactions involving various ions such as H^+, Na^+, K^+ and Li^+, which contributes to higher specific capacitances [1, 6, 7]. Transition metal oxides as well have some disadvantages like low electrical conductivity and poor cycling performance. Therefore, efforts are still going on to improve performance of supercapacitors.

In spite of many binary metal oxides, mixed metal oxides and higher order metal oxides have been reported to demonstrate better pseudocapacitive performance because they possess multiple oxidation states that enable numerous redox reactions and combined contribution from all metal ions. A number of ternary metal oxides such as $NiCo_2O_4$ [7–9], $MnCo_2O_4$ [10], $NiMoO_4$ [11], $NiFe_2O_4$ [12], $CoMn_2O_4$ [13], $CuCo_2O_4$ [14], $LiNiO_2$ [15], $LiCoO_2$ [16] and $Li_4Ti_5O_{12}$ [17], have been used as electrode material for pseudocapacitors. Transition metal vanadium oxides and vanadates such as $Ni_3(VO_4)_2$ [18], $Co_3V_2O_8$ and $Ni_3V_2O_8$ [19] have been reported as a new class of electrode material for

pseudocapacitors owing to their multistep reductions and more electron transfer upon intercalation. In particular, lithium-based vanadates got significant attention owing to their capability of storing lithium by the ion intercalation-extraction mechanism [20]. Detailed examination on such materials indicate that an element having a low oxidation state plays foremost role in the generation of pseudocapacitance, while an element having a high oxidation state has a trivial influence on the pseudocapacitance [21]. Recently, LiV_3O_8 nanosheet has been reported as a pseudocapacitor electrode material with an initial specific capacitance of 288 F g^{-1} and a capacitance of 98 F g^{-1} after 100 cycles in 1 M $LiNO_3$ electrolyte [22]. Lithium nickel vanadate ($LiNiVO_4$) has been recognized as a promising cathode material for lithium ion batteries. $LiNiVO_4$ possess an AB_2O_4 inverse spinel structure in which Li^+ ions and Ni^{2+} ions equally reside in octahedral sites, and V^{5+} ions occupy the tetrahedrally coordinated sites. Lithium ion present in the octahedral site exhibits a reversible electrochemical intercalation-extraction process [23, 24]. However, the exploitation of $LiNiVO_4$ as electrode material for pseudocapacitors has not yet been investigated.

The electrochemical properties of a material depend, amongst others, on the synthesis method and on the size and shape of the particles. So far, $LiNiVO_4$ crystallites were synthesized by means of various techniques including solid state reaction [25], hydrothermal method [26] and sol-gel method [24], to improve their electrochemical properties. Besides, nano-sized materials offer enhanced electrochemical performance because of short path length for ion and electron transport, and the ability to take advantage of surface properties [7]. In particular, the Faradaic process at the surface of the material, referred to as pseudocapacitive effect, becomes prominent at nanoscale dimensions.

In this paper, the size dependent pseudocapacitive behaviour of $LiNiVO_4$ electrode has been investigated. Here, we prepared $LiNiVO_4$ particles of (1) nanoscale range by hydrothermal synthesis; (2) conventional microsized particles by mechanochemical synthesis. The synthesized $LiNiVO_4$ electrode materials have been characterized by X-ray diffraction (XRD), Fourier-transform infrared (FT-IR) spectroscopy, thermogravimetric analysis (TGA), differential thermal analysis (DTA), field emission scanning electron microscopy (FESEM) and energy dispersive X-ray (EDS) analysis. The size effect of $LiNiVO_4$ on lithium ion intercalation-deintercalation reaction is evaluated by cyclic voltammetry, electrochemical impedance spectroscopy and constant current charge-discharge measurements. The intercalation pseudocapacitance is further confirmed by X-ray photoelectron spectroscopy (XPS) measurements. The electrochemical evaluation resulted a specific capacitance of 456.56 F g^{-1} at a current density of 0.5 A g^{-1} with superior cycling stability.

Experimental

The chemicals employed for $LiNiVO_4$ synthesis and electrode fabrication includes lithium nitrate ($LiNO_3$, 99.99% purity), nickel nitrate ($Ni(NO_3)_2.6H_2O$, 99.999% purity), ammonium metavanadate (NH_4VO_3, 99.99% purity), polyvinylidene fluoride (average Mw ~ 534,000) and N-methyl-2-pyrrolidone (anhydrous, 99.5%), and all were purchased from Sigma Aldrich. Carbon black (Super P) was purchased from Alfa Aesar. All chemicals were used as received, without any further purification.

Mechanochemical synthesis

3 mmol $LiNO_3$, 3 mmol $Ni(NO_3)_2.6H_2O$ and 3 mmol NH_4VO_3 were weighed, ball milled with 30 mL deionized water for 12 h, using yittrium stabilized zirconia balls in a polyethylene jar. The dried powders were heated at 400 °C for 4 h and ground by using an agate mortar and pestle. Then, the powders were re-heated to 800 °C for 6 h.

Hydrothermal synthesis

2 mmol $LiNO_3$, 2 mmol $Ni(NO_3)_2.6H_2O$ and 2 mmol NH_4VO_3 were dissolved in 30 mL deionized water at 80 °C. The precursor solution was transferred into a 40 mL Teflon-lined autoclave and maintained at 200 °C for 12 h. The brown yellow precipitate obtained was thoroughly washed with deionized water and ethanol to remove ions possibly remaining in the final products and dried at 80 °C in the air. The powder obtained was further annealed at 400 °C in air for 2 h to increase crystallinity.

Structural and electrochemical characterizations

The crystal phase and average crystallite size of prepared $LiNiVO_4$ were analysed using X-ray diffractometry (XRD, PANalytical X'Pert Pro) with Cu-Kα radiation (λ = 1.5406 Å). The functional groups were identified using Fourier-transform infrared (FT-IR, PerkinElmer Spectrum 100) spectra recorded employing the KBr pellet method. A thermogravimetric analysis (TGA) and a differential thermal analysis (DTA) analysis were carried out to evaluate thermal stability (Hitachi STA7300 Thermal analysis system), under inert atmosphere employing a heating rate of 10 °C min^{-1}. The morphology and microstructure of the electrode materials were observed by scanning electron microscopy (HRSEM, FEI Quanta FEG 200). The elemental composition was indentified using energy dispersive X-ray spectrometry (EDS).

Individual electrodes were used for electrochemical evaluation of $LiNiVO_4$ obtained by both mechanochemical (S-$LiNiVO_4$) and hydrothermal (H-$LiNiVO_4$) syntheses. The electrodes were prepared by mixing $LiNiVO_4$ active material,

carbon black (Super P), and polyvinylidene fluoride (PVDF) with N-methyl-2-pyrrolidone (NMP) in the mass ratio of 80:10:10. Then, the slurry was pressed onto the nickel foam, current collector (1 cm × 1 cm) and dried at 60 °C for 12 h in vacuum. The electrochemical characterization of the electrodes were performed in a three-electrode cell using 1 M LiOH aqueous solution as electrolyte, in which platinum mesh and Ag/AgCl electrode were employed as the counter and the reference electrode, respectively. Cyclic voltammetry (CV), galvanostatic charge-discharge (GCD) and electrochemical impedance spectroscopy (EIS) were performed using a PGSTAT302N electrochemical work station (Metrohm Autolab, Netherlands). The CV curves were measured in a potential range of − 0.2 to 0.6 V (vs. Ag/AgCl). The EIS was measured at electrode potential of 0 V vs. Ag/AgCl, a perturbation potential of 5 mV and a frequency range of 0.1 Hz to 100 kHz. The electrochemical capacitance was investigated through GCD measurements. The X-ray photoelectron spectroscopy (XPS, Kratos-Analytical Axis Ultra X-ray photoelectron spectrophotometer with a monochromatic Al-K_α-X-ray source.) measurements of electrode materials were carried out to estimate the various chemical states of the bonded atoms. The specific capacitance (F g^{-1}) of the $LiNiVO_4$ electrode was calculated from charge-discharge curves according to the following equation:

$$C = \frac{I \times \Delta t}{m \times \Delta V}$$

where I (A) is the constant discharge current density, Δt (s) is the discharge time, ΔV (V) is the discharge voltage excluding the IR drop and m (g) is the mass of the active material coated on the electrode.

Results and discussion

Structural and morphological characterizations

The crystal structure and phase purity of $LiNiVO_4$ synthesized via mechanochemical and hydrothermal reaction were characterized by powder XRD, as shown in Fig. 1a. $LiNiVO_4$ exhibited characteristic diffraction peaks at 2θ = 18.60°, 30.90°, 36.44°, 44.14°, 54.84°, 58.42°, 64.09°, 73.04° and 76.80°, corresponding to the crystal planes of (111), (220), (311), (400), (422), (511), (440), (620) and (533), respectively. It is clear that all intense diffraction peaks corresponds to cubic phase of $LiNiVO_4$ and Fd3m (227) space group (JCPDS No. 38-1395), without any collateral peaks. The diffraction peaks indexed as (311) and (111) planes are characteristics of an inverse spinel structure [27]. The presence of sharp diffraction peaks indicates high degree of crystallinity of the prepared sample. The XRD patterns are almost identical for $LiNiVO_4$ synthesized by both methods. However, the diffraction peaks becomes broad for H-$LiNiVO_4$, implying smaller crystallite size, which can shorten the ion diffusion pathways and reduce the charge-transfer resistance. The average crystallite sizes of $LiNiVO_4$ synthesized by both methods were determined from the full width at half maximum (FWHM) of the x-ray diffraction peak using Scherrer equation:

$$D = \frac{K\,\lambda}{\beta\,Cos\,\theta}$$

where D is the average crystallite size, K is the Scherrer constant, 0.94 for cubic crystal structure, λ is the wavelength of Cu-Kα radiations (1.5406 Å), β is the full width at half maximum of the peak corresponding to (311) plane in radian and θ is the angle obtained from 2θ value corresponding to the maximum intensity peak in XRD pattern. The calculated value for the average crystallite size of the S-$LiNiVO_4$ and H-$LiNiVO_4$ powders are 551.16 and 65 nm, respectively.

FT-IR spectrum of $LiNiVO_4$ in the wave number range of 400 to 1200 cm^{-1} is presented in Fig. 1b. The absorption band observed at 852.57, 764.13 and 607.06 cm^{-1} are assigned to stretching vibrations of VO_4 tetrahedrons. The bands at 750 to 400 cm^{-1} region are largely associated with the vibrations of NiO_6 and LiO_6 octahedral units or the bending vibrations of VO_4 tetrahedron. The two absorption band sited around 1091.06 and 1030.22 cm^{-1} belongs to an asymmetric stretching vibrational mode of Ni-O bonds in NiO_6 octahedron [28]. The two weak bands around 455.28 and 426.50 cm^{-1} are assigned to asymmetric stretching vibrations caused by Li-O bond of LiO_6 octahedron.

Thermal studies were carried out in order to determine the thermal stability and decomposition profile of the sample. We examined TGA and DTA under argon atmosphere in a temperature range from 25 to 750 °C with a heating rate of 10 °C min^{-1} (Fig. 1c, d). The observed initial weight loss below 100 °C is attributed to the evaporation of residual water. The next weight loss noticed in the wide temperature range is due to the decomposition of lithium nitrate and ammonium metavanadate, which takes place at the melting point of both raw materials. The decomposition process stops for S-$LiNiVO_4$ and H-$LiNiVO_4$ at nearly 600 and 500 °C, respectively. The degree of weight loss until the weight stabilizes in micro-sized S-$LiNiVO_4$ (9.02%) is greater than that of nano-sized H-$LiNiVO_4$ (1.75%). The greater weight loss in the S-$LiNiVO_4$ can be attributed to the enthalpic gain due to weak bonding between constituent atoms as well as entropic gain obtained by liberating the water molecules [29]. The peak position in the DTA curve matches with the temperature of the first derivative of the TGA curve, where structural changes occur.

Figure 2a, b depicts the FESEM micrographs of the $LiNiVO_4$ powder synthesized by mechanochemical reaction and hydrothermal reaction, respectively. As seen in the figure, irregular/defected cubic-like micro-sized (~ 500 nm) $LiNiVO_4$ particles are obtained from mechanochemical method and

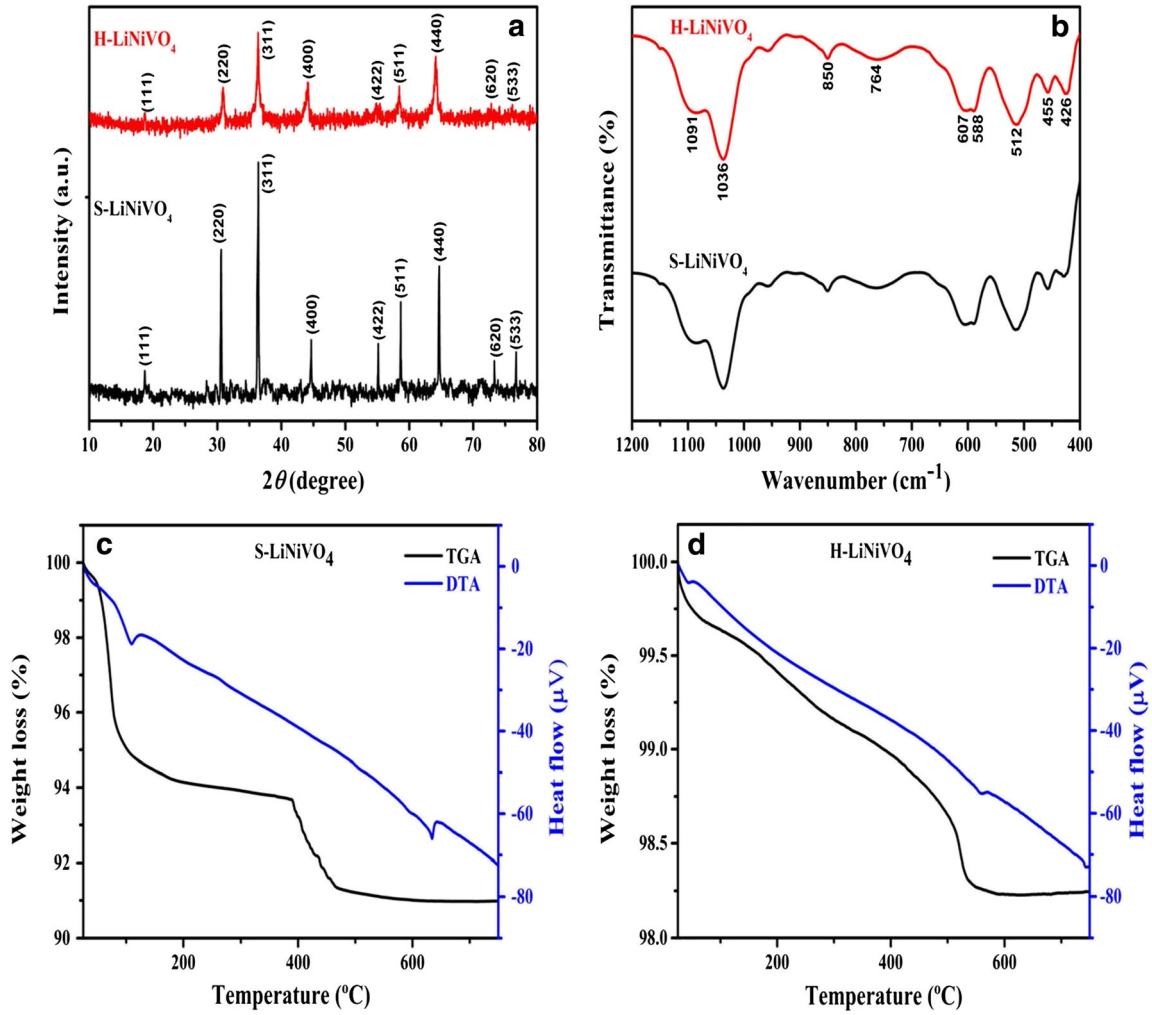

Fig. 1 **a** X-ray diffraction patterns of S-$LiNiVO_4$ and H-$LiNiVO_4$. **b** FT-IR spectrum of S-$LiNiVO_4$ and H-$LiNiVO_4$. TGA and DTA curves of **c** S-$LiNiVO_4$, **d** H-$LiNiVO_4$

defect free nano-sized (~ 60 nm) particles from hydrothermal method. Elemental composition of $LiNiVO_4$ is confirmed using energy dispersive X-ray spectrometry (EDS), which is shown in Fig. 2c, d. EDS analysis demonstrated the presence of Ni, V and oxygen with an average ratio of 1:1 for Ni:V.

Electrochemical evaluation

Figure 3a, b shows the current-voltage (CV) curves of material synthesized by mechanochemical and hydrothermal reaction in 1 M LiOH electrolyte at various potential sweep rate. Two strong redox peaks suggests the reversible electrochemical oxidation (Li extraction) and reduction (Li insertion) of $LiNiVO_4$ electrode material. The large redox peaks arising due to Faradaic redox reactions indicate that the capacitance characteristic of $LiNiVO_4$ electrode is of typical pseudocapacitance. The peak current rises with increase in the potential sweep rate, indicating rapid Faradaic redox reactions and increased rates of electronic and ionic transport [30]. Comparative CV studies of $LiNiVO_4$ micro and nanostructures (Fig. 3c) indicate that the area of the CV curve for the $LiNiVO_4$ nanostructure is larger than that of the $LiNiVO_4$ microstructure, which is obviously due to the higher surface area, thereby more number of active sites in the former. The difference in redox peak positions between micro and nano-structured $LiNiVO_4$ electrodes may be ascribed to the differences in the individual electronic transition, which may be influenced by the morphological differences. Investigation of CV can be further considered as an efficient tool to explain electrode kinetics in micro and nano-structured $LiNiVO_4$. In the case of S-$LiNiVO_4$ electrode, the redox peak does not exhibits significant shift in their positions with increase in potential sweep rate, indicating a typical pseudocapacitive Li^+ intercalation/deintercalation behaviour without phase transformation. Therefore, the peak current varies linearly with the potential sweep rate. On the other hand, a slight shift in the redox peak position is observed for H-$LiNiVO_4$ electrode with increased potential sweep rate. This can be described by the existence of two capacitive processes, namely interface-related pseudocapacitive contribution arising from

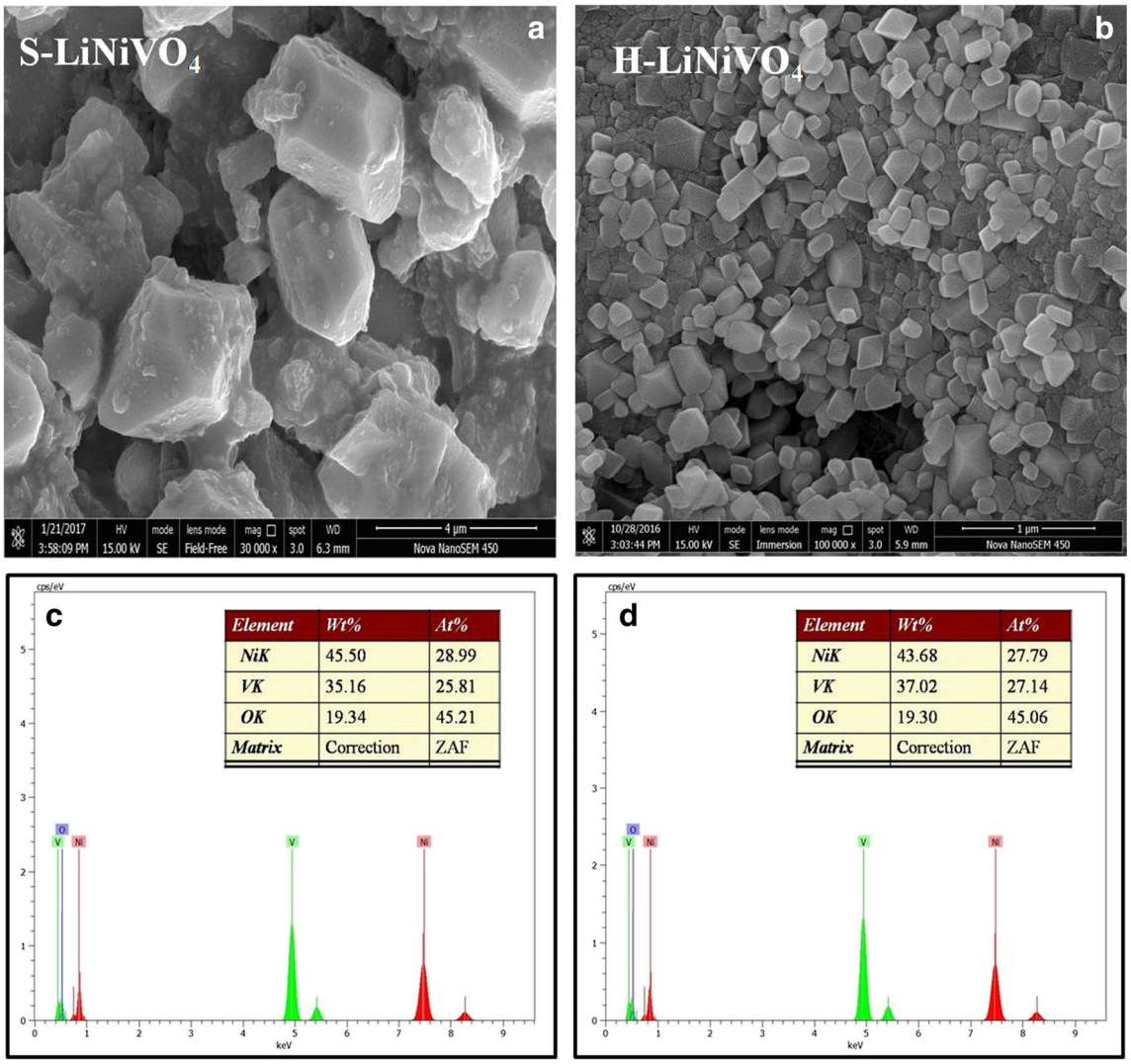

Fig. 2 FESEM images of **a** S-$LiNiVO_4$, **b** H-$LiNiVO_4$ and EDS pattern of **c** S-$LiNiVO_4$, **d** H-$LiNiVO_4$

the large active surface area of nanocrystalline structure and diffusion-controlled Li^+ intercalation reaction [31, 32]. Hence, the pseudocapacitive charge storage mechanism of $LiNiVO_4$ via the intercalation of lithium ions in an aqueous electrolyte is proposed as follows:

$$LiNiVO_4 + xLi^+ + xe^- \leftrightarrow Li_{1+x}NiVO_4$$

In order to substantiate the CV results, the electrochemical impedance spectroscopy (EIS) analysis was carried out for $LiNiVO_4$ electrodes. Nyquist plots of both micro and nano-sized $LiNiVO_4$ electrodes are shown in Fig. 3d. The straight line at low-frequency region represents Warburg impedance, which results from the ion diffusion at the electrode-electrolyte interface. The line at lower frequencies which is parallel to imaginary axis, indicate the desired pseudocapacitive behaviour. Inset of Fig. 3b shows the equivalent circuit of the impedance curve obtained using the ZSimpWin software. The fitted EIS data contains elements of bulk solution resistance (R_s), charge-transfer resistance (R_{ct}), constant phase element (*CPE*) to account for double layer capacitance, Warburg diffusion element (W_o) and a pseudocapacitive element (C_p) from the redox processes at the electrode. The equivalent series resistance (R_s) of the electrodes can be obtained from the high frequency intersection of EIS Nyquist plot in the real axis. It is found that H-$LiNiVO_4$ has reduced R_s value compared with S-$LiNiVO_4$ electrode. The decrease in the R_s value could be attributed to the small particle size of electrode, which shortens the ion diffusion path length and thereby enhance the mobility of ions in the electrolyte. Moreover, the absence of semicircle in high frequency region of impedance plot implies negligible charge-transfer resistance. From the results calculated using ZSimpWin software, R_{ct} of S-$LiNiVO_4$ and H-$LiNiVO_4$ electrodes are 0.02 and 0.01 Ω, respectively. A slightly reduced value of R_{ct} originates from the quick charge-transfer process occurring in the pseudocapacitive H-$LiNiVO_4$ electrode owing to short electron path length.

The charge storage capacity of $LiNiVO_4$ electrode was further investigated using galvanostatic charge-discharge

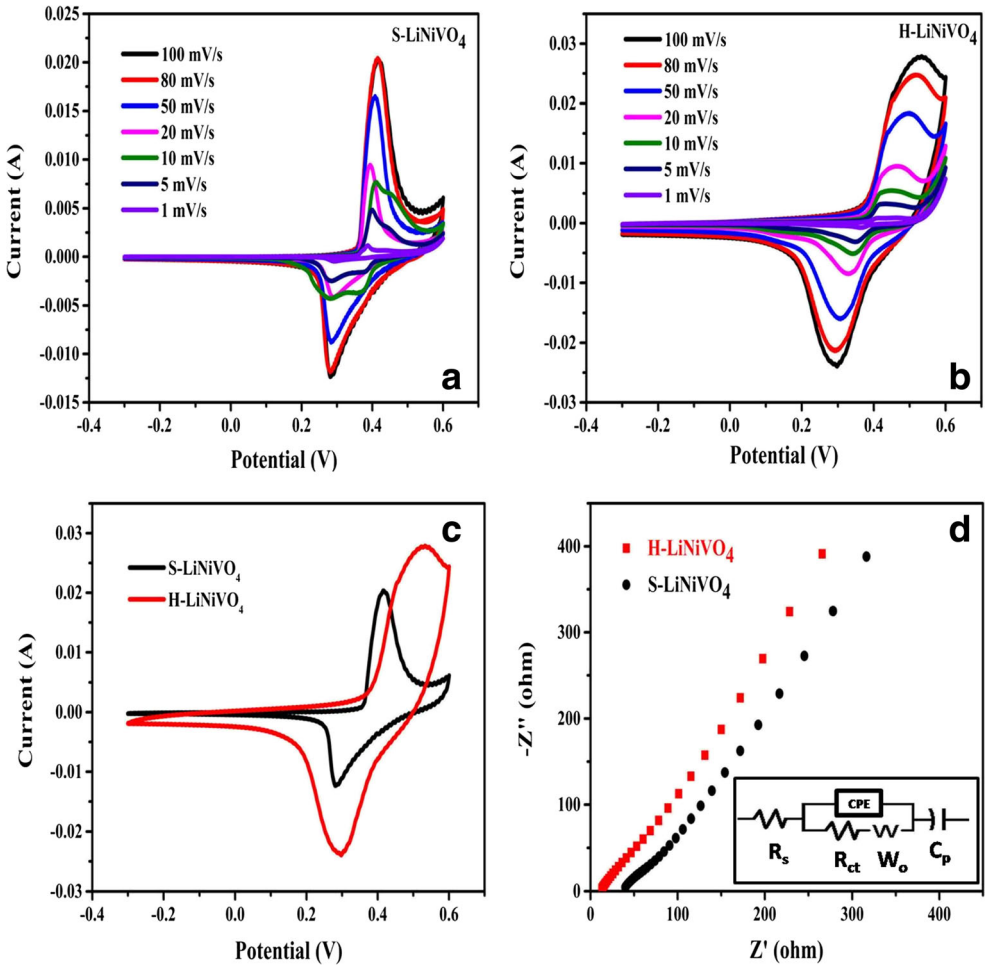

Fig. 3 CV curves of $LiNiVO_4$ electrode material at various potential sweep rates in 1 M LiOH electrolyte solution: **a** S-$LiNiVO_4$, **b** H-$LiNiVO_4$, **c** CV curves of S-$LiNiVO_4$ and H-$LiNiVO_4$ electrodes at a potential sweep rate of 100 mV s^{-1} and **d** Nyquist plots of S-$LiNiVO_4$ and H-$LiNiVO_4$ electrodes (*inset*: fitted equivalent circuit)

measurements in the potential range of −0.2 to 0.52 V. Figure 4a, b displays the discharge behaviours of both micro and nano-sized $LiNiVO_4$ electrodes at different current densities. A comparative charge-discharge curve of the $LiNiVO_4$ electrodes as well as bare Ni foam is depicted in Fig. 4c. The H-$LiNiVO_4$ electrode showed longer charge-discharge time than the S-$LiNiVO_4$ electrode, demonstrate higher specific capacitance. The maximum specific capacitance reaches 212.70 and 456 F g^{-1} for S-$LiNiVO_4$ and H-$LiNiVO_4$, respectively, at a current density of 0.5 A g^{-1}. The high capacitance of H-$LiNiVO_4$ can be mainly ascribed to the nano size of $LiNiVO_4$. The nanocrystalline structure of H-$LiNiVO_4$ not only provide a fast ion transport path and a large active surface area, but also enhances the accessibility of LiOH electrolyte and therefore, promotes the ion transport within the electrode. Figure 4d shows the variation of specific capacitance with applied current. The decrease in the specific capacitance with increasing discharge current could be attributed to the increase in potential drop as well as insufficient Faradaic redox reactions at higher currents. Further, the long term cycling stability of the both electrode material were investigated at the current density of 1 A g^{-1} (Fig. 5a, b). After 1000 continuous charge-discharge cycles, $LiNiVO_4$ electrodes exhibited excellent cycling stability with no sign of capacitance degradation. Capacitance retention of 99.04 and 99.60% was obtained for S-$LiNiVO_4$ and H-$LiNiVO_4$ electrodes, respectively, which is better than those of other lithium-based and nickel-based vanadates, such as LiV_3O_8 nanosheet (34.12% retention after 100 cycles) [22], $Ni_3V_2O_8$ nanoflakes (73.0% after 1000 cycles) [21]. The excellent cycle stability of the electrodes may be attributed to the morphological and structural stability of $LiNiVO_4$. The inverse spinel structure of $LiNiVO_4$ electrode, which enables ion intercalation/extraction between electrode and electrolyte leads to Faradic reaction, resulting in better electrochemical performance.

XPS measurements of $LiNiVO_4$ electrode material were carried out before and after cycling, which provide critical evidence about the excellent electrochemical performance. The XPS survey spectra of S-$LiNiVO_4$ and H-$LiNiVO_4$ before and after cycling (Fig. 6a, b) confirm the distinct peaks of Li 1s, Ni 2p, V 2p and O 1s. The XPS peaks C 1s and F 1s originated from Super P and PVDF employed during electrode coating process. The XPS peaks in survey spectra of both micro and nano-structured $LiNiVO_4$ electrodes before cycling are in good

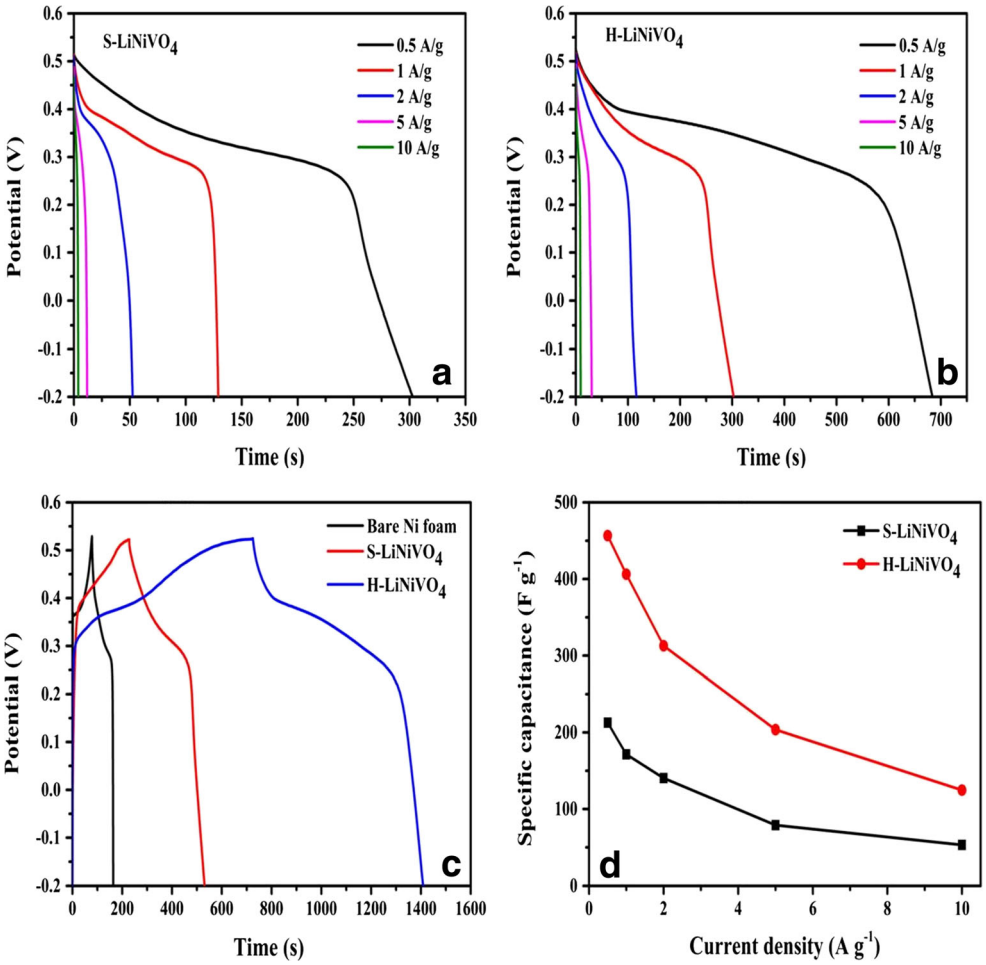

Fig. 4 Constant current discharge curves of $LiNiVO_4$ electrode material at various current densities: **a** S-$LiNiVO_4$, **b** H-$LiNiVO_4$, **c** charge-discharge curves of bare Ni foam, S-$LiNiVO_4$ and H-$LiNiVO_4$ at a current density of 0.5 A g^{-1} and **d** specific capacitances at various discharge current densities

agreement with the electrode after 1000 cycles, which leads to the conclusion that there is no change in the oxidation states of $LiNiVO_4$ constituents upon cycling. Figure 6c, d shows the comparative XPS core level spectrum of Ni 2p, which contain two major peaks with binding energies at 856.9 and 863.1 eV correspond to Ni $2p_{3/2}$ and Ni $2p_{1/2}$, respectively. It is obvious that the Ni 2p peaks hardly change even after cycling. This realization verifies that pseudocapacitance behaviour in

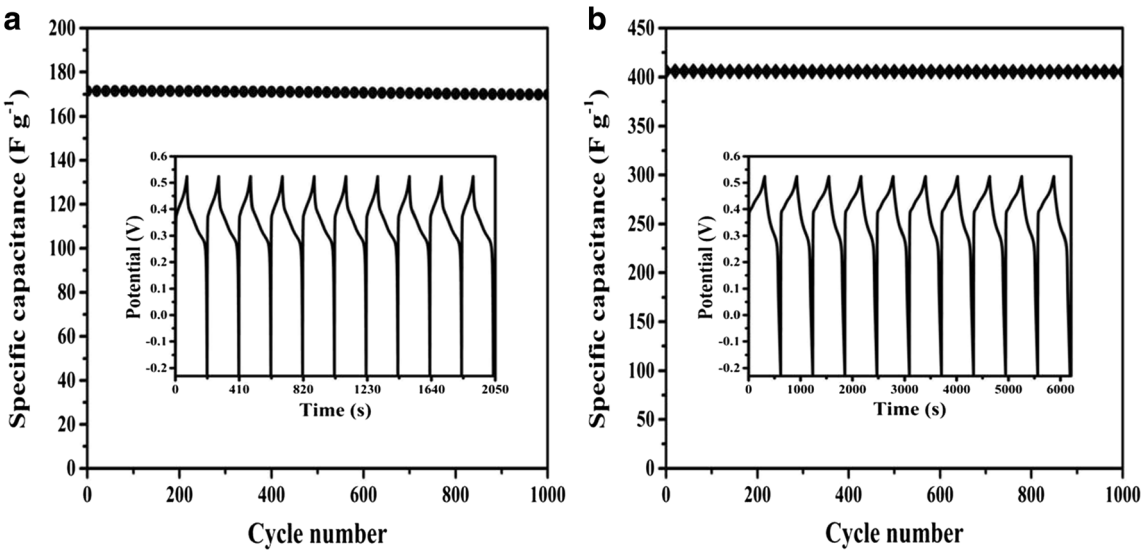

Fig. 5 Charge-discharge cycling at a current density of 1 A g^{-1}: **a** S-$LiNiVO_4$ and **b** H-$LiNiVO_4$ electrodes (*inset*: charge-discharge curves for first 10 cycles)

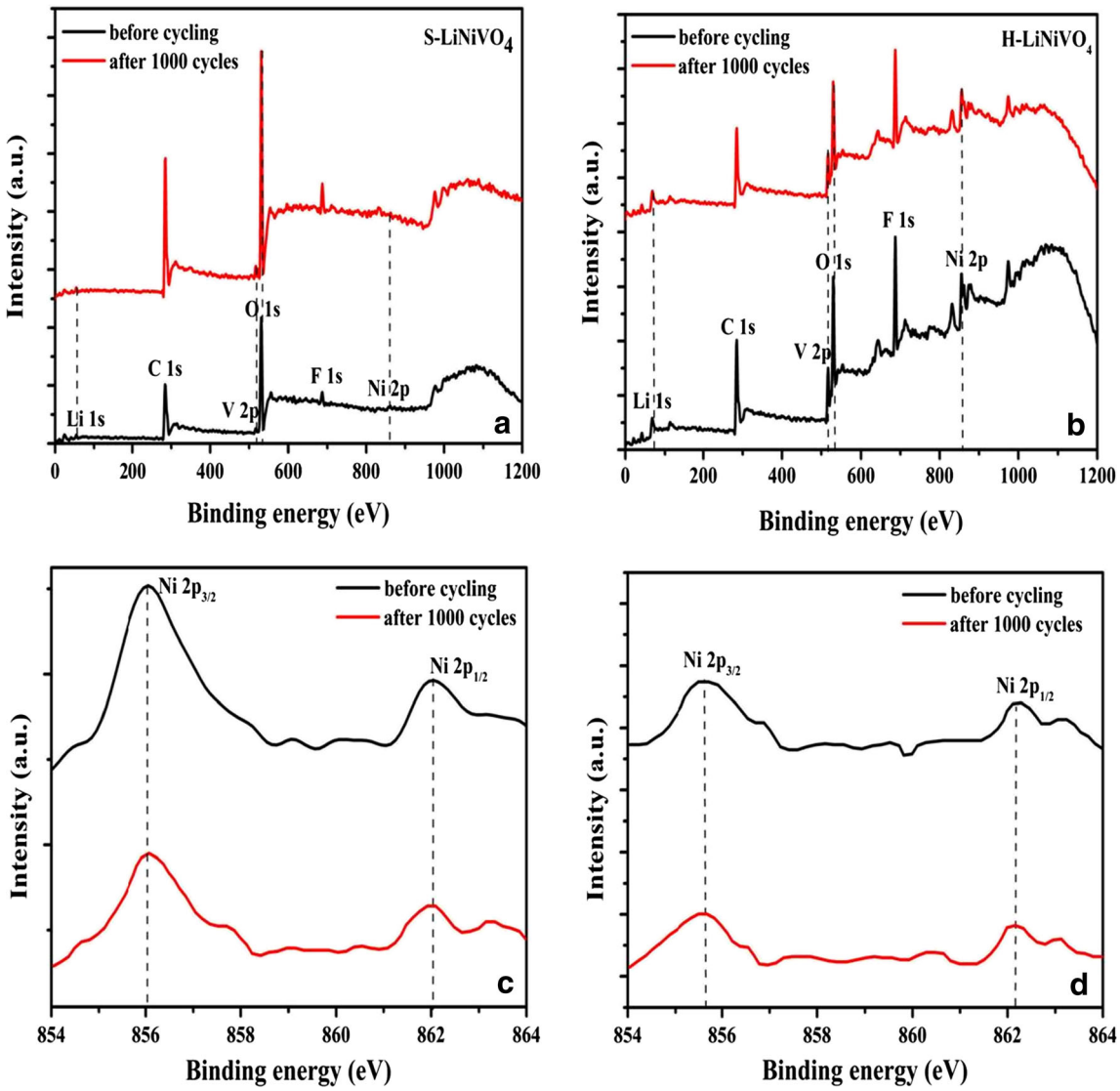

Fig. 6 XPS survey spectra of **a** S-$LiNiVO_4$ electrode before and after cycling and **b** H-$LiNiVO_4$ electrode before and after cycling. Comparative XPS core level spectrum of Ni 2p: **c** S-$LiNiVO_4$ electrode before and after cycling and **d** H-$LiNiVO_4$ electrode before and after cycling

$LiNiVO_4$ electrode is purely Li^+ intercalation/de-intercalation, which further confirms the proposed intercalation mechanism.

The excellent electrochemical performance of the H-$LiNiVO_4$ electrode material can be attributed to the nanocrystalline structure of $LiNiVO_4$ beneficial for the utilization of the pseudocapacitive active material and Li^+ intercalation/deintercalation reaction between active electrode materials and electrolyte resulting in elevated capacitance. Overall, this investigation establishes that $LiNiVO_4$ brings a new class of vanadate exhibiting Li^+ intercalation pseudocapacitance.

Conclusion

This work has demonstrated the pseudocapacitive behaviour of $LiNiVO_4$ electrode material synthesized via mechanochemical reaction and hydrothermal reaction. The influence of crystallite size on supercapacitor performance is evaluated. Even though, the chemical composition of S-$LiNiVO_4$ and H-$LiNiVO_4$ are identical, H-$LiNiVO_4$ exhibited higher specific capacitance due to their small crystallite size and more redox active sites, providing a fast ion transport path and enhanced electrolyte accessibility. The nanocrystalline H-$LiNiVO_4$ electrode could achieve a high specific capacitance of 456.56 F g^{-1}, which is significantly greater than micro-sized S-$LiNiVO_4$ (212.70 F g^{-1}) at a current density of 0.5 A g^{-1}. The $LiNiVO_4$ electrode exhibits excellent capacitance retention of 99.04 and 99.60% for S-$LiNiVO_4$ and H-$LiNiVO_4$, respectively, even after 1000 cycles owing to the unique structural features. Therefore, the application of $LiNiVO_4$ as electrochemical pseudocapacitor electrode material is demonstrated for first time in literature pave the way for a new class of pseudocapacitive electrode material. The

electrochemical performance of $LiNiVO_4$ material may be further improved by altering the synthesis route, varying the electrolytes, such as organic electrolytes and ionic liquids and dispersing in conductive carbon or polymeric materials.

Acknowledgements The authors acknowledge the financial support from Indian Institute of Space Science and Technology (IIST) Trivandrum, NIIST Trivandrum for XRD, SAIF IIT Madras for SEM-EDS analysis and ACNSMM Kochi for XPS analysis.

References

1. Long CL, Jiang LL, Wei T, Yan J, Fan ZJ (2014) High-performance asymmetric supercapacitors with lithium intercalation reaction using metal oxide-based composites as electrode materials. J Mater Chem A 2:16678–16686
2. Xiang C, Li M, Zhi M, Manivannan A, Wu N (2013) A reduced graphene oxide/Co3O4 composite for supercapacitor electrode. J Power Sources 226:65–70
3. Wang Y, Guo J, Wang T, Shao J, Wang D, Yang Y-W (2015) Mesoporous transition metal oxides for supercapacitors. Nanomaterials 5:1667–1689
4. Yuan C, Bin WH, Xie Y, Lou XW (2014) Mixed transition-metal oxides: design, synthesis, and energy-related applications. Angew Chemie - Int Ed 53:1488–1504
5. Pan Y, Gao H, Zhang M, Li L, Wang Z (2017) Facile synthesis of ZnCo2O4 micro-flowers and micro-sheets on Ni foam for pseudocapacitor electrodes. J Alloys Compd 702:381–387
6. Long C, Wei T, Yan J, Jiang L, Fan Z (2013) Supercapacitors based on graphene-supported iron nanosheets as negative electrode materials. ACS Nano 7:11325–11332
7. Salunkhe RR, Jang K, Yu H, Yu S, Ganesh T, Han S-H, Ahn H (2011) Chemical synthesis and electrochemical analysis of nickel cobaltite nanostructures for supercapacitor applications. J Alloys Compd 509:6677–6682
8. Gupta RK, Candler J, Palchoudhury S, Ramasamy K, Gupta BK (2015) Flexible and high performance supercapacitors based on NiCo2O4for wide temperature range applications. Sci Rep 5:15265
9. Jokar E, zad AI, Shahrokhian S (2015) Synthesis and characterization of NiCo2O4 nanorods for preparation of supercapacitor electrodes. J Solid State Electrochem 19:269–274
10. Pettong T, Iamprasertkun P, Krittayavathananon A, Sukha P, Sirisinudomkit P, Seubsai A, Chareonpanich M, Kongkachuichay P, Limtrakul J, Sawangphruk M (2016) High-performance asymmetric supercapacitors of $MnCo_2O_4$ nanofibers and N-doped reduced graphene oxide aerogel. ACS Appl Mater Interfaces 8:34045–34053
11. Peng S, Li L, Bin WH, Madhavi S, Lou XWD (2015) Controlled growth of $NiMoO_4$ nanosheet and nanorod arrays on various conductive substrates as advanced electrodes for asymmetric supercapacitors. Adv Energy Mater 5:1401172
12. Yu Z-Y, Chen L-F, Yu S-H, Yu M, Xie S, Ling Y, Liang C, Tong Y, Li Y, Gong L, Chen J, Tong Y, Zhou J, Wang ZL (2014) Growth of NiFe2O4 nanoparticles on carbon cloth for high performance flexible supercapacitors. J Mater Chem A 2:10889
13. Yunyun F, Xu L, Wankun Z, Yuxuan Z, Yunhan Y, Honglin Q, Xuetang X, Fan W (2015) Spinel CoMn2O4 nanosheet arrays grown on nickel foam for high-performance supercapacitor electrode. Appl Surf Sci 357:2013–2021
14. Vijayakumar S, Lee S-H, Ryu K-S (2015) Hierarchical CuCo2O4 nanobelts as a supercapacitor electrode with high areal and specific capacitance. Electrochim Acta 182:979–986
15. Gulzar U, Goriparti S, Miele E, Li T, Maidecchi G, Toma A, De Angelis F, Capiglia C, Zaccaria RP (2016) Next-generation textiles: from embedded supercapacitors to lithium ion batteries. J Mater Chem A 4:16771–16800
16. Xu Y, Ding L, Zhong T, Han X, Jiao L, Yuan H, Wang Y (2015) Novel application of LiCoO2 as a high-performance candidate material for supercapacitor. J Energy Chem 24:193–198
17. Khairy M, Faisal K, Mousa MA (2017) High-performance hybrid supercapacitor based on pure and doped Li4Ti5O12 and graphene. J Solid State Electrochem 21:873–882
18. Zhang Y, Liu Y, Chen J, Guo Q, Wang T, Pang H (2014) Cobalt vanadium oxide thin nanoplates: primary electrochemical capacitor application. Sci Rep 4:3537–3543
19. Cheng F, Chen J (2011) Transition metal vanadium oxides and vanadate materials for lithium batteries. J Mater Chem 21:9841
20. Long C, Jiang L, Wei T, Yan J, Fan Z, Yang ZP, Wang ZL, Wang ZL, Jing X, Xie S, Lee YH, Tong Y, Zhou J, Wang ZL (2014) High-performance asymmetric supercapacitors with lithium intercalation reaction using metal oxide-based composites as electrode materials. J Mater Chem A 2:16678–16686
21. Liu M-C, Kong L-B, Kang L, Li X, Walsh FC, Xing M, Lu C, Ma X-J, Luo Y-C, Broholm C, Ramirez AP (2014) Synthesis and characterization of M3V2O8 (M = Ni or Co) based nanostructures: a new family of high performance pseudocapacitive materials. J Mater Chem A 2:4919
22. Zheng J, Zhang Y, Wang N, Zhao Y, Tian F, Meng C (2016) Facile synthesis and characterization of LiV3O8 with sheet-like morphology for high-performance supercapacitors. Mater Lett 171:240–243
23. Zhao Z, Ma J, Xie L, Tian H, Zhou J, Hu Y, Huang X, Wu P, Dai J, Zhu Z, Wang H, Chen H (2005) A low-temperature molten salt synthesis of LiNiVO4 cathode material for lithium ion batteries. J Am Ceram Soc 88:2622–2624
24. Prakash D, Masuda Y, Sanjeeviraja C (2013) Synthesis and structure refinement studies of LiNiVO4 electrode material for lithium rechargeable batteries. Ionics (Kiel) 19:17–23
25. Lu C-H, Liou S-J (1999) Fabrication and microstructure of lithium nickel vanadium oxide prepared by solid-state reaction. Ceram Int 25:431–436
26. Lu C-H, Liou S-J (2000) Hydrothermal preparation of nanometer lithium nickel vanadium oxide powder at low temperature. Mater Sci Eng B 75:38–42
27. Li X, Wei YJ, Ehrenberg H, Liu DL, Zhan SY, Wang CZ, Chen G (2009) X-ray diffraction and Raman scattering studies of Li+/e−−extracted inverse spinel LiNiVO4. J Alloys Compd 471:L26–L28
28. Bhuvaneswari MS, Selvasekarapandian S, Kamishima O, Kawamura J, Hattori T (2005) Vibrational analysis of lithium nickel vanadate. J Power Sources 139:279–283
29. Kim S-I, Lee J-S, Ahn H-J, Song H-K, Jang J-H (2013) Facile route to an efficient NiO supercapacitor with a three-dimensional nanonetwork morphology. ACS Appl Mater Interfaces 5:1596–1603
30. Zhang W-B, Kong L-B, Ma X-J, Luo Y-C, Kang L (2014) Nickel vanadate and nickel oxide nanohybrid on nickel foam as pseudocapacitive electrodes for electrochemical capacitors. RSC Adv 4:41772–41777
31. Augustyn V, Simon P, Dunn B, Grüner G, Regan BC, Dunn B, Lu Y, Che S, Chapman T, Jaworski R, Dimitrijevic NM, Podsiadlo P, Johnson CS, Rajh T (2014) Pseudocapacitive oxide materials for high-rate electrochemical energy storage. Energy Environ Sci 7:1597. doi:10.1039/c3ee44164d
32. Wang Y, Song Y, Xia Y, Taberna PL, Simon P, Grey CP, Simon P, Grey CP, Wu DH, Zhu HW, Jin HJ, Stach EA, Ruoff RS (2016) Electrochemical capacitors: mechanism, materials, systems, characterization and applications. Chem Soc Rev 45:5925–5950. doi:10.1039/C5CS00580A